INSTITUTE OF PHYSICS PUBLISHING NANOTECHNOLOGY
Nanotechnology 17 (2006) 3613–3621 doi:10.1088/0957-4484/17/14/042

In situ structure characterization of airborne carbon nanofibres by a tandem mobility–mass analysis

Bon Ki Ku[1,4], Mark S Emery[2], Andrew D Maynard[3], Mark R Stolzenburg[2] and Peter H McMurry[2]

[1] Centers for Disease Control and Prevention (CDC), National Institute for Occupational Safety and Health (NIOSH), 4676 Columbia Parkway, MS-R3, Cincinnati, OH 45226, USA
[2] Particle Technology Laboratory, Department of Mechanical Engineering, University of Minnesota, 111 Church St. S.E., Minneapolis, MN 55455, USA
[3] Woodrow Wilson International Center for Scholars, Project on Emerging Nanotechnologies, One Woodrow Wilson Plaza, 1300 Pennsylvania Avenue NW, Washington DC 20004, USA

E-mail: BKu@cdc.gov

Received 5 April 2006, in final form 19 May 2006
Published 26 June 2006
Online at stacks.iop.org/Nano/17/3613

Abstract
Carbon nanofibres aerosolized by the agitation of as-produced commercial powder have been characterized *in situ* by using the differential mobility analyser–aerosol particle mass analyser (DMA–APM) method to determine their structural properties such as the effective density and fractal dimension for toxicology study. The effective density of the aerosolized carbon nanofibres decreased from 1.2 to 0.4 g cm^{-3} as the mobility diameters increased from 100 to 700 nm, indicating that the carbon nanofibres had open structures with an overall void that increased with increasing diameter, due to increased agglomeration of the nanofibres. This was confirmed by transmission electron microscopy (TEM) observation, showing that 100 nm mobility diameter nanofibres were predominantly single fibres, while doubly or triply attached fibres were seen at mobility diameters of 200 and 400 nm. Effective densities calculated using Cox's theory were in reasonable agreement with experimental values. The mass fractal dimension of the carbon nanofibres was found to be 2.38 over the size range measured and higher than that of single-walled carbon nanotubes (SWCNTs), suggesting that the carbon nanofibres have more compact structure than SWCNTs.

1. Introduction

The production of engineered nanostructured materials from nanometre-diameter particles (nanoparticles) raises concern over the potential health hazards presented by such particles when manufacturing and handling them in the workplace [1–3]. Carbon nanotubes/ nanofibres represent a unique class of engineered nanomaterial that may have applications in fields such as novel electronic devices and high-strength materials [4–6]. While desired properties of engineered nanomaterials including carbon nanotubes/nanofibres are predominantly associated with their size, shape, and nanometre-scale structure (physically and chemically), it is anticipated that the size distribution, agglomerate state, shape, chemical composition, surface area and surface chemistry of these nanomaterials may be important physicochemical properties that could lead to adverse health effects [2]. Previous studies have shown that the biological response is associated with the nanoscale structure and composition of single-walled carbon nanotube (SWCNT) particles [1, 7, 8]. In addition, airborne SWCNTs generated by the mechanical agitation of commercial powders have shown particle size-dependent physicochemical structure [9]. Like SWCNTs, carbon nanofibres have recently become a focal point of research, with special interest as the fibre diameters approach the nanometer range. Although some research on the

[4] Author to whom any correspondence should be addressed.

toxicity of carbon nanotubes/nanofibres has been performed using different generation and test methods, relatively little is known of the physical or chemical characteristics of these nanomaterials or which properties of the materials will be closely associated with toxicity. Furthermore, the range of approaches and methods used to reach conclusions regarding the toxicity of carbon nanotubes/nanofibres nanomaterials has led to different results [2]. This inconsistency indicates that these nanomaterials need to be well characterized physically and chemically before evaluating potential nanomaterial toxicity in order to get comparable results. In addition, the variety and complexity of nanomaterials suggests that the level of characterization appropriate to toxicity tests should be commensurately more sophisticated.

A differential mobility analyser–aerosol particle mass analyser (DMA–APM) method was developed by McMurry and his colleagues [10, 11] and used to measure the effective density of diesel soot particles and urban atmospheric aerosols. This technique involves the sequential classification of gas-borne particles according to mobility by the DMA and mass by the APM. Together, this information can be used to infer the effective density (mass divided by volume based on the mobility equivalent diameter). When the particles are also examined in an electron microscope, it is possible to determine the inherent material density and the dynamic shape factor as well [12]. This approach is especially useful for obtaining information on irregularly shaped particles.

In this study we used the DMA–APM method to characterize the airborne carbon nanofibre structure and morphology in real-time. Specifically, the effective density and fractal dimension of airborne carbon nanofibres (Pyrograf-III, Type PR-24, Grade LHT, Applied Sciences Inc.) with a single mobility diameter ranging from 100 to 700 nm were measured. The as-produced carbon nanofibres were aerosolized using a vortex shaker-based generation system [3] and the effective densities measured by the DMA–APM method were compared with those calculated using aerodynamic diameters obtained from Cox's theory [13]. In addition, carbon nanofibre particle shape and aspect ratio as a function of mobility diameter were examined using transmission electron microscopy (TEM) analysis to provide valuable qualitative insights into the relationship between particle morphology and particle properties such as the effective density and fractal dimension.

2. Theory

2.1. *Effective density and fractal dimension*

Several definitions for effective density have been well discussed by DeCarlo *et al* [14]. The effective density measured in our study is defined as the particle mass divided by the particle volume based on mobility diameter [10, 11]. The effective density depends on material density, particle shape and porosity, and is an important physical property of a particle, because it affects particle transport properties and provides information about particle structure and morphology [14, 15]. The effective density can be obtained by measuring the mass of a particle with a known mobility diameter. Recent experimental and theoretical studies showed that the density of spherical particles of known composition can be measured to within ~5–6% using the APM [10, 16].

The fractal dimension is also an important particle property for determining the structure of agglomerate particles [14]. The mass fractal dimension D_f can be expressed as follows [11, 17]:

$$m \sim (d_m)^{D_f} \tag{1}$$

where m is the particle mass and d_m is the mobility equivalent diameter. Therefore, the mass fractal dimension of carbon nanofibres corresponds to the slope in a log–log plot of mass versus mobility diameter, with a value of three describing spherical particles.

2.2. *Calculation of effective density based on aerodynamic diameter obtained from Cox's theory*

Cox's theory [13] allows a direct computation of aerodynamic diameter, d_a, for a cylinder or fibre moving in a viscous fluid. For motion perpendicular to the major axis of a fibre, aerodynamic diameter is

$$d_{a,\perp} = d_f \left(\frac{9\rho}{8\rho_0} \{\ln(2\beta) + 0.193\} \right)^{1/2}, \tag{2}$$

and for motion parallel to its major axis,

$$d_{a,\parallel} = d_f \left(\frac{9\rho}{4\rho_0} \{\ln(2\beta) - 0.807\} \right)^{1/2}, \tag{3}$$

where β is the aspect ratio of a cylinder (fibre length/fibre diameter), ρ is the fibre material density (we assume a value of 2.0 g cm^{-3} for carbon nanofibres), ρ_0 is the unit density (1 g cm^{-3}), and d_f is the fibre diameter. β and d_f of single mobility carbon fibres were determined by TEM analysis in our study. Because the orientation of the particles is constantly changing due to Brownian rotation [18], the average aerodynamic diameter from the above equations was used ($1/3d_{a,\parallel} + 2/3d_{a,\perp}$; $d_{a,\perp}$ is preferred during gravitational acceleration [18, 19]). Combining the aerodynamic diameter calculated by Cox's theory with the relationship between d_m and d_a used in Park *et al*'s work [11], the theoretical effective density is obtained.

3. Experimental methods

A schematic diagram of the experimental setup used is shown in figure 1. Pyrograf®-III material (Type PR-24, Grade LHT, Applied Sciences Inc.) was placed in a test tube and shaken using a laboratory vortex shaker (Vortex Genie 2, Model G560, Scientific Industries Inc., Bohemia, NY, USA). HEPA-filtered air was passed through the test tube at 0.3–1.0 l min^{-1} and entrained aerosol particles that were transported through an impactor (0.0457 cm diameter nozzle, part number 1502295, TSI Inc.) to a scanning mobility particle sizer (SMPS 3936, TSI Inc.). The size distributions of polydisperse carbon nanofibre aerosols that were generated were measured using an SMPS and Aerodynamic Particle Sizer (APS 3321, TSI Inc.). Monodisperse particles were generated using a DMA (3081, TSI Inc.) to select the carbon nanofibres of a predetermined mobility diameter for TEM sampling and APM measurement.

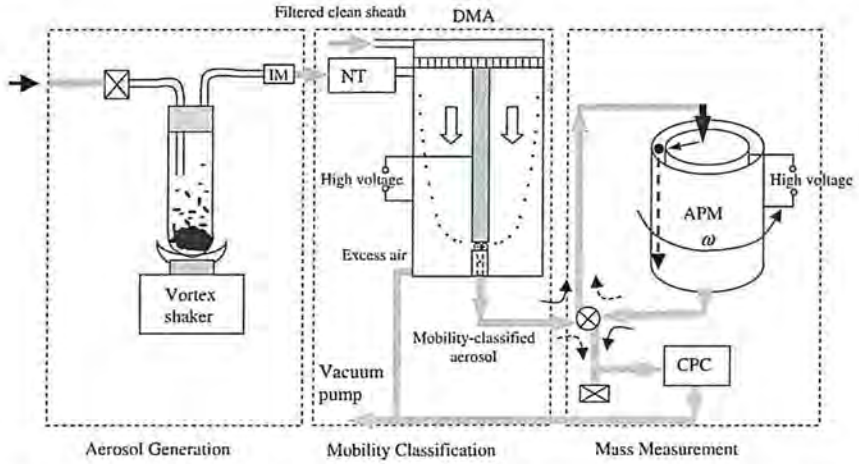

Figure 1. Experimental setup for structure characterization of airborne nanofibres by a tandem mobility–mass analysis (DMA: differential mobility analyser; APM: aerosol particle mass analyser; CPC: condensation particle counter; IM: impactor; NT: neutralizer).

The DMA, based on electrical mobility separation of particles [20], extracts particles with a narrow range of mobilities out of an input flow including particles of many sizes and charges. The DMA-classified particles were sampled for TEM analysis using an impactor-based electrostatic precipitator [21].

3.1. APM

The APM consists of two concentric cylinders that rotate together at a controlled rate. The outer cylinder (63 mm in radius) is maintained at ground, and a classifying voltage is applied to the inner cylinder (60 mm in radius). Charged particles introduced axially into the small annular gap experience centrifugal and electrostatic forces, which act in opposite directions. The concentration of particles downstream from the APM is measured as the classifying voltage is varied. The concentrations pass through a peak value at the voltage where the centrifugal and electrostatic forces are balanced [10, 11]. Note that the APM measures the true particle mass, independently of other particle properties such as density, shape and size. Further details on the APM are described in previous papers [10, 11, 22].

3.2. DMA-APM measurement

Carbon nanofibres aerosolized by a vortex shaker were introduced to a Po-210 neutralizer to provide a Boltzmann equilibrium charge distribution before entering the DMA. Then, the DMA-classified monodisperse carbon nanofibre particles were sampled through the APM rotating at a specific speed. Measurements were carried out with particles having mobility sizes ranging from 100 to 700 nm in 50 nm increments. For each size, the particle mass was measured by varying the APM voltage while it was rotating at a speed fixed. For each APM voltage, the particle number concentration was measured by the CPC (TSI 3760), and the peak APM voltage corresponding to the peak mass for the mobility-selected particles was determined. We used this peak voltage to determine the 'average' particle mass of each mobility size. In order to obtain the best APM resolution, the theoretical code developed by Emery [16] was used to select the APM parameters such as rotational speed and voltage scanning range. For particles larger than 100 nm, mobility-classified particles typically contain both singly and multiply charged particles. Early work showed that singly and doubly charged particles of a given single mobility are cleanly separated by the APM [10]. For example, the APM voltage required to classify doubly charged particles of a given density and mobility is 2.48 times the value required for singly charged particles of 309 nm mobility size.

3.3. DMA-TEM analysis

Particles of three different mobility sizes (100, 200, and 400 nm) were classified by the DMA and sampled on TEM grids by an impactor-based electrostatic precipitator [21]. About 30–50 TEM carbon nanofibre particles were taken and used to measure fibre diameters and length-to-diameter ratios (aspect ratio). These were used to calculate aerodynamic diameters based on Cox' theory [13] and also to investigate size-dependent structures. Moderately overlapped straight nanofibres were selected and considered for nanofibre diameter and aspect ratio measurements. As much as 15% of the 200 nm particles and 20% of the 400 nm particles were excluded, since they were severely overlapped on the collection substrate.

4. Results and discussion

4.1. Structure characterization of airborne carbon nanofibres

The size distribution of carbon nanofibres generated by agitation of as-produced commercial Pyrograf-III powder and measured by SMPS and APS is shown in figure 2. Most of the carbon nanofibres generated were larger than 60 nm in mobility diameter, with the modal mobility diameter occurring at around 250 nm, while modal aerodynamic diameter was about 700 nm. There is a discontinuous region between the mobility and aerodynamic diameter distributions, indicating

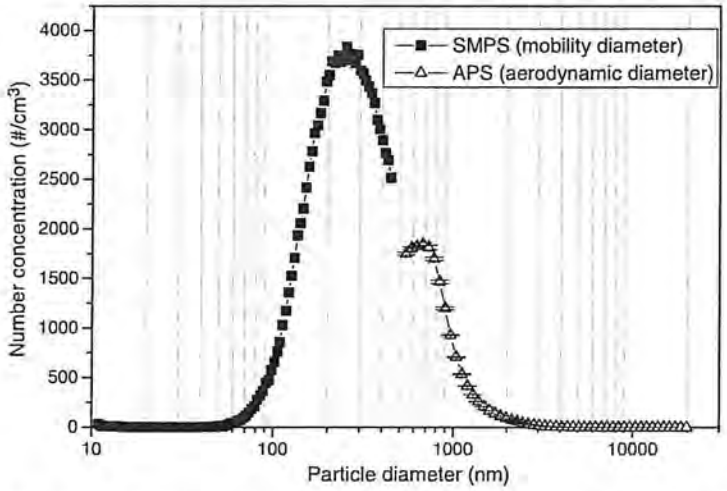

Figure 2. Size distribution of carbon nanofibre particles generated by a vortex shaker and measured by SMPS and APS. Note that the discontinuity between the SMPS and APS distributions occurs because the SMPS measures the mobility diameter and the APS measures the aerodynamic diameter, which are significantly different for these particles.

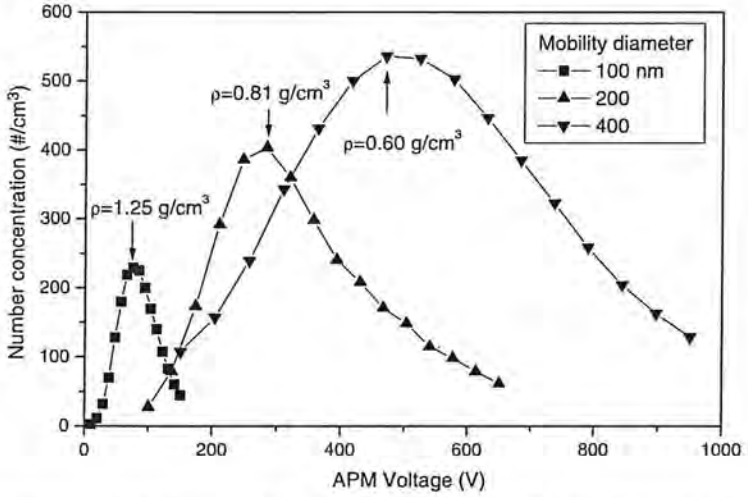

Figure 3. Number concentrations measured downstream of the APM as a function of the APM classifying voltage for three different mobility size particles (100, 200 and 400 nm). Each data point was obtained by averaging five samples under the same conditions.

that carbon nanofibres are obviously non-spherical and have density different from unity (1 g cm^{-3}) which was assumed in the APS measurement. Further investigation of the aerodynamic size distribution using an electrical low-pressure impactor (ELPI) confirmed the aerodynamic modal diameter (not shown here).

Figure 3 shows number concentrations measured downstream from the APM as a function of the APM classifying voltage for three representative mobility-classified particle sizes. Each data point was obtained by averaging five samples taken under the same conditions. Successive measurements were found to be very reproducible and consistent. For each mobility size, the mean effective density was calculated using the voltage corresponding to the peak in the plot of number versus voltage. As particle size increased from 100 to 400 nm, the effective density decreased from around 1.2–0.6 g cm^{-3}, indicating that the carbon nanofibres had open structures with an overall void that increased with increasing diameter. There are several phenomena that could lead to the observed decrease in effective density, including a more open structure and a greater void space within the nanofibres themselves. According to the TEM analysis of internal void fractions of individual fibres, defined as a ratio of internal void volume to fibre volume, the internal void fraction showed little variation for three different mobility diameter fibres, approximately 0.25–0.28. Therefore, the lower effective density is more likely to be caused by the agglomeration of fibres. This was confirmed by TEM analysis, which showed that the 100 nm mobility diameter nanofibres were predominantly single fibres, while doubly or triply attached fibres were seen at mobility diameters of 200 and

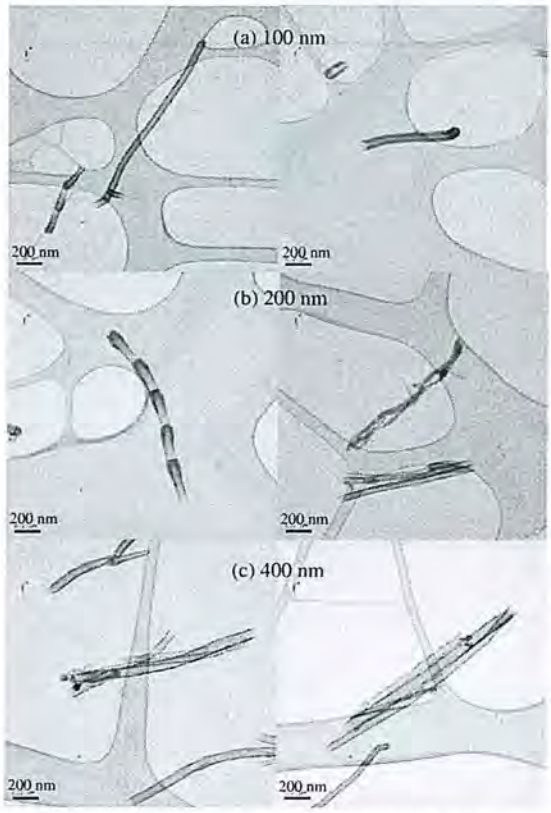

Figure 4. TEM micrographs of Pyrograf-III particles of 100 nm (a), 200 nm (b) and 400 nm (c) mobility diameter. All the images shown were taken at the same magnification.

400 nm, as shown in figure 4. TEM analysis also showed particles produced from Pyrograf-III powder often consisted of agglomerates of multiple single fibres. This led to increased fluffiness of the nanofibre bundles for larger carbon nanofibres, due to their agglomerated structures. From a health perspective, the particle agglomeration state is very important because it may have a significant impact on biological activity. Weakly attached carbon fibres may de-agglomerate in the lung following inhalation, while strongly bonded fibres are expected to retain their structures.

Figure 5 represents the effective density distributions calculated based on Cox's theory [13] and the relationship between mobility diameter and aerodynamic diameter [11] with fibre diameters and aspect ratios obtained from TEM analysis. Each data in figure 5 was fitted assuming a Gaussian distribution. Calculated mean effective densities of 100, 200 and 400 nm nanofibres were 1.83 g cm^{-3}, 1.08 g cm^{-3} and 0.57 g cm^{-3}, respectively, which are in fair agreement with those measured by the APM in figure 3.

Number concentration distributions in figure 3 tend to become broader with increasing mobility diameter for the APM-measured data. This can be explained by the transfer functions of the DMA and APM (i.e. the probability that particles are transported through the instruments). Emery has recently shown that the APM resolution, that is, peak narrowness, in the number-APM voltage distribution inherently increases with increasing APM speed and voltage at a fixed aerosol flow rate [16]. In our study, higher APM speed and lower range voltage were used for smaller size particles. Based on calculation of peak narrowness using Emery's code [16], APM resolution for 400 nm particles is predicted to be 0.9 times that for 100 nm particles, which is qualitatively consistent with our observation that peak widths

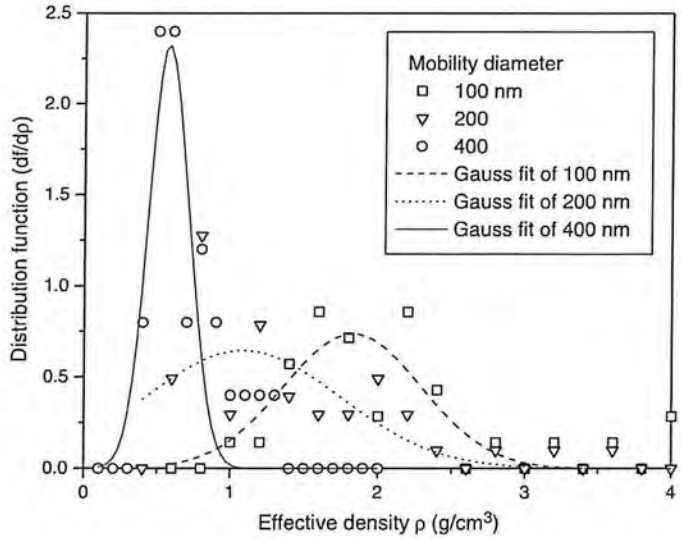

Figure 5. Effective density distributions calculated by Cox's theory and relationship between mobility diameter and aerodynamic diameter for three different mobility size particles. The distribution function on the y-axis is the fraction (f) of particles with a given effective density divided by density bin width. Each data set was fitted using a Gaussian fit and each mean effective density was 1.83 g cm^{-3}, 1.08 g cm^{-3} and 0.57 g cm^{-3}, respectively for 100, 200 and 400 nm.

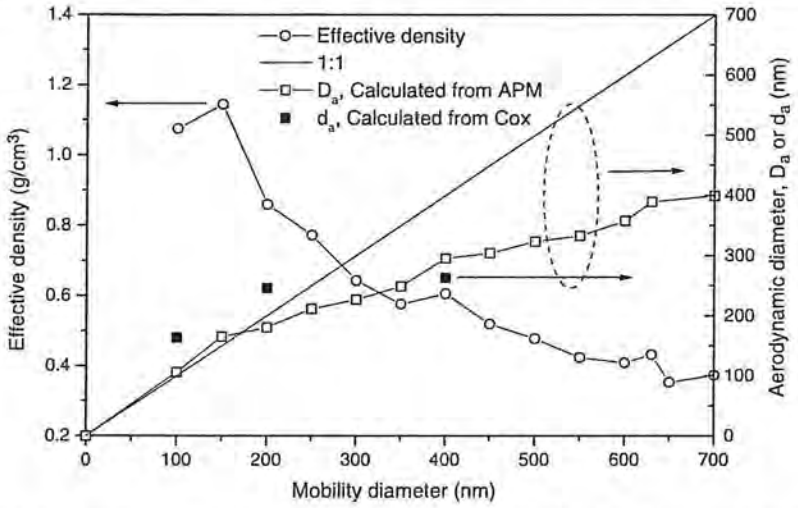

Figure 6. Effective density and aerodynamic diameter of carbon nanofibres as a function of mobility diameter. Effective density data was obtained by averaging three samples from the APM.

Table 1. Effective densities, aerodynamic diameters and masses of single-mobility carbon nanofibre particles in the 100–700 nm size range.

Mobility diameter d_m (nm)	Effective density[a] ρ_{eff} (g cm^{-3})	Aerodynamic diameter[b] d_a (nm)	Particle mass m (fg)
100	1.08–1.25[c]	105.8	0.56–0.63
150	1.14	165.0	2.02
200	0.86	180.6	3.60
250	0.77	211.3	6.32
300	0.64	226.7	9.10
350	0.58	248.5	12.93
400	0.61	295.4	20.3
450	0.52	304.2	24.78
500	0.48	323.2	31.24
550	0.42	332.8	36.92
600	0.41	357.8	46.3
630	0.43	389.3	56.6
700	0.37	399.3	67.04

[a] Measured by APM.

[b] Calculated by using equation (1) in [11] with known d_m and m.

[c] The effective density for 100 nm particles has a relatively large uncertainty to low concentration of this size particles (see figure 2).

increased as mobility size increased. However, dispersion of the number concentrations for a given mobility particles was found to be significantly broader than that for oil droplets of a similar mass, possibly reflecting of variation in particle effective density and structure and/or orientation in the DMA or APM [15].

Figure 6 represents the effective densities of carbon nanofibres with sizes ranging from 100 up to 700 nm. Each density was obtained by averaging three data samples under the same condition for each particle size. The effective density of carbon nanofibres gradually decreases as the mobility diameter increases, with maximum values of about 1.2 g cm^{-3} for particles of 100–150 nm mobility diameters, decreasing to 0.4 g cm^{-3} for about 700 nm. These results indicate that carbon nanofibres become more compact as their size decreases. Interestingly, the effective density decreased markedly as the particle size increased from 150 to 200 nm. In this size range, the effective density also dropped below unit density. Based on our TEM observations (figure 4), this sudden change is likely due, in part, to the onset of agglomeration among nanofibres, which resulted in some doubly and triply attached fibres. Aerosol particles of 100 nm mobility diameter showed little evidence for multiply attached fibres in their structure as shown in figure 4(a).

Figure 6 also includes aerodynamic diameter variation as a function of mobility diameter. The aerodynamic diameter was calculated using the relationship between d_m and d_a used in Park *et al*'s work [11] combined with measured particle mass and mobility size. The difference between aerodynamic diameter and mobility diameter increases with increasing mobility diameter because the effective density decreases as the mobility diameter increases. For particles smaller than 200 nm mobility size, the aerodynamic diameter is a little bit larger than mobility diameter, because densities exceed 1 g cm^{-3}. The aerodynamic diameters calculated by Cox's theory for particles with mobility sizes of 100, 200 and 400 nm are also shown in figure 6, approximately confirming the relationship between aerodynamic diameter and mobility diameter that the aerodynamic diameter becomes smaller than mobility diameter somewhere between 200 and 400 nm. With the information of TEM images for 100, 200 and 400 nm sizes, nanofibre true density (defined as mass from APM divided by volume from TEM data) and dynamic shape factor (refer to [10]) were calculated. Nanofibres with mobility size of 400 nm were found to have a mean true density of 1.96 g cm^{-3}, which is close to the value of 2.0 g cm^{-3}, we assumed and a mean dynamic shape factor of 1.59 ± 0.21, while 100 and 200 nm nanofibres were observed to have a density lower than 2.0 g cm^{-3}. Effective density, aerodynamic diameter and mass as a function of mobility diameter for fibres over the size ranging from 100 to 700 nm are summarized in table 1.

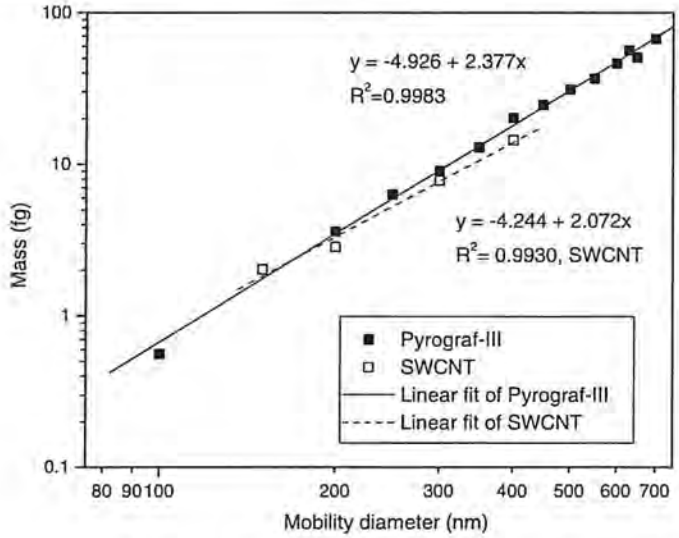

Figure 7. Log–log plot of mass versus mobility diameter. The mass fractal dimension is equal to the slope of the linear fit. Note that the nanofibre particles of Pyrograf-III material have a higher fractal dimension than SWCNTs, indicating carbon nanofibres are structurally more compact than the SWCNTs.

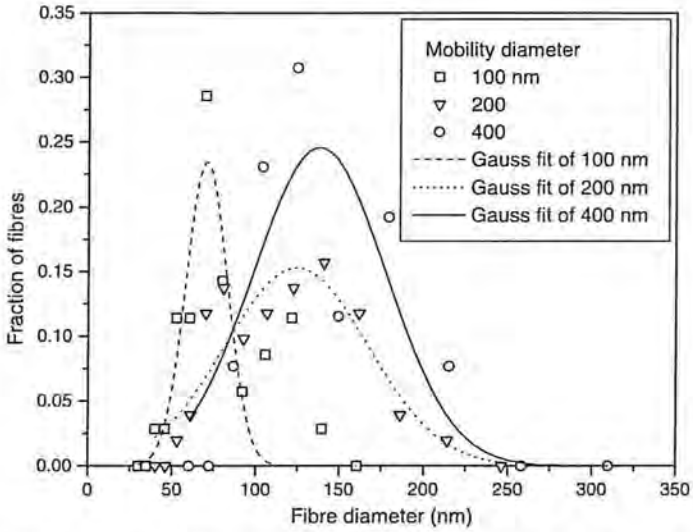

Figure 8. Fibre diameter distribution measured by TEM analysis for three mobility diameters. Fibre diameter increases as mobility diameter increases, showing a fair correlation over the size range from 100 to 400 nm. The mean nanofibre diameters for 100, 200 and 400 nm mobility sizes were 70 nm (standard deviation 25 nm), 124 nm (86 nm) and 138 nm (79 nm), respectively.

Particle mass measurement, combined with mobility classification, also allowed us to measure the mass fractal dimension over the size range from 100 to 700 nm. Figure 7 shows the mass versus mobility diameter in a log–log plot; the slope of the linear fit in figure 7 equals the mass fractal dimension. Data for SWCNT and Pyrograf®-III are shown in this figure. Note that both materials exhibit a good power-law relationships between the mass and mobility diameter. The mass fractal dimension of Pyrograf®-III carbon nanofibres was found to be 2.38, while that for SWCNTs was 2.07, clearly indicating that carbon nanofibres have a more compact structure than SWCNTs. Previous studies [3, 9] showed that the SWCNT particles consist of bundles of individual nanotubes (single molecules) self-assembled into ropes (from approximately about 2 nm to greater than 50 nm in diameter) which can splay apart and form much larger expanded structures. However, the nanofibres were found to be much larger in diameter in our study. Figure 8 shows that the nanofibre diameters range from about 40 nm up to 200 nm, depending on mobility size. The mean nanofibre diameters for 100, 200 nm and 400 nm mobility sizes were 70 nm (standard deviation 25 nm), 124 nm (86 nm) and 138 nm

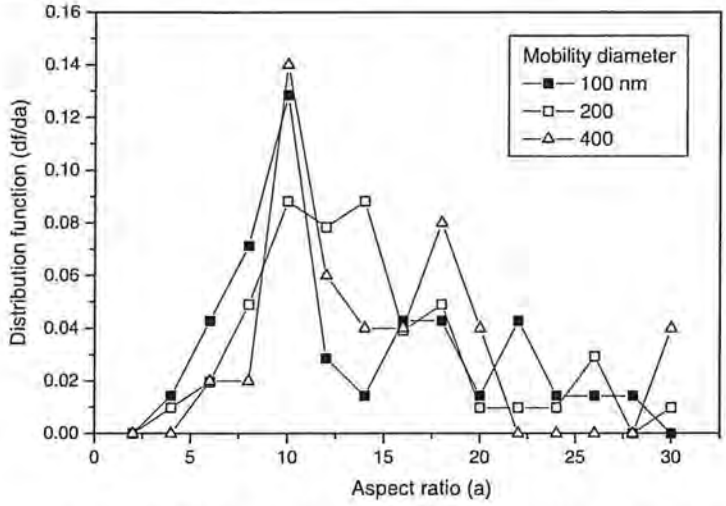

Figure 9. Aspect ratio distribution measured by TEM analysis for three different mobility size fibres. The distribution function on y-axis was is equal to the fraction (f) of particles with a given aspect ratio divided by aspect ratio bin width. Fibre aspect ratios appear to show a mode around 10 for three mobility sizes.

(79 nm), respectively, showing somewhat broad distributions of fibre diameters. As was shown in figure 4, individual fibres were clearly visible and did not self-organize into well-defined bundles, but rather tended to attach more randomly to each other as matted material, which is consistent with the result of relatively high fractal dimension or compact structure for carbon nanofibres. Recently, Maynard *et al* have shown that 150 nm mobility diameter SWCNTs have nanoropes in their structure [9], which contributes to the lower fractal dimension of SWCNTs observed in our study.

TEM analysis also provided information about fibre aspect ratios defined as ratios of fibre length to diameter. Figure 9 shows that, for all three sizes investigated in this study, the carbon nanofibres generated a range from 2 to 30, with a mode of 10 and an average of 13 to 14. The independence of the aspect ratio on the mobility size suggests that the fibre length and diameter increase at the same rate as the mobility diameter. It is not clear why the three different mobility-classified fibres had a similar aspect ratio at about 10.

4.2. The importance and possible impact of nanomaterial characterization by the DMA–APM method in the field of nanotechnology

A recent review of engineered nanomaterial toxicity screening tests has emphasized the importance of structure as well as chemistry in determining potential hazard, and stressed the need to fully characterize the physicochemical nature of materials under study [2]. We have, for the first time, characterized in detail the structure of carbon nanofibres representing a unique class of engineered nanomaterial by using the DMA–APM method, which is dependent on the particle size. In addition, we have demonstrated the use of the DMA–APM method combined with TEM analysis to obtain information on the relationship between the particle morphology and particle properties of irregularly shaped nanoparticles such as carbon nanofibres. Our work indicates that the DMA–APM method should be generic to any airborne nanomaterial, as long as serial mobility and mass measurements are possible. Exposures to engineered nanomaterials when manufacturing and handling such materials in the workplace are predicted to increase due to the advent of nanotechnology [23]. For this reason, the DMA–APM method is anticipated to be widely applicable to determining the physicochemical properties of airborne nanostructured materials, which may be relevant to potential health hazard.

5. Conclusions

The DMA–APM technique has been applied to *in situ* structure characterization of airborne carbon nanofibres. Effective density and fractal dimension were obtained directly from measurements of nanofibre mobility size and mass for a range of fibre sizes. The effective densities of the carbon nanofibres decreased with increasing mobility diameter, indicating that they have open structures with an overall void that increased with increasing diameter, due to the increased agglomeration of the nanofibres. A comparison of mass fractal dimension of the nanofibres with that of SWCNTs also showed that the nanofibres have a more compact structure than SWCNTs. Because the structure affects transport and locations of deposition within the respiratory system and may affect toxicology, it is important to characterize structures of airborne materials used for toxicology studies.

Disclaimer

The mention of any company or product does not constitute an endorsement by the Centers for Disease Control and Prevention. The findings and conclusions in this report are those of the authors and do not necessarily represent the views of the National Institute for Occupational Safety and Health.

References

[1] Shvedova A A *et al* 2005 Unusual inflammatory and fibrogenic pulmonary responses to single-walled carbon nanotubes in mice *Am. J. Physiol.-Lung Cell Mol. Physiol.* **289** L698–708

[2] Oberdörster G *et al* 2005 Principles for characterizing the potential human health effects from exposure to nanomaterials: elements of a screening strategy *Part. Fibre Toxicol.* **2** 1–110 (doi:10.1186/1743-8977-2-8)

[3] Maynard A D, Baron P A, Foley M, Shvedova A A, Kisin E R and Castranova V 2004 Exposure to carbon nanotube material: Aerosol release during the handling of unrefined single walled carbon nanotube material *J. Toxicol. Environ. Health* **67** 87–107

[4] Subramoney S 1998 Novel nanocarbons—structure, properties, and potential applications *Adv. Mater.* **10** 1157–71

[5] Sinnott S B and Andrews R 2001 Carbon nanotubes: synthesis, properties, and applications *Crit. Rev. Solid State Mater. Sci.* **26** 145–249

[6] Applied Sciences Inc., http://www.apsci.com/ppi-pyro3.html

[7] Shvedova A A, Kisin E R, Murray A R, Gandelsman V Z, Maynard A D, Baron P A and Castranova V 2003 Exposure to carbon nanotube material: Assessment of the biological effects of nanotube materials using human keratinocyte cells *J. Toxicol. Environ. Health* **66** 1909–26

[8] Warheit D B, Laurence B R, Reed K L, Roach D H, Reynolds G A M and Webb T R 2004 Comparative pulmonary toxicity assessment of single-wall carbon nanotubes in rats *Toxicol. Sci.* **77** 117–25

[9] Maynard A D, Ku B K, Emery M S, Stolzenburg M and McMurry P H 2005 Measuring particle size-dependent physicochemical structure in airborne single walled carbon nanotube agglomerates, personal communication

[10] McMurry P H, Wang X, Park K and Ehara K 2002 The relationship between mass and mobility for atmospheric particles: a new technique for measuring particle density *Aerosol Sci. Technol.* **36** 227–38

[11] Park K, Cao F, Kittelson D B and McMurry P H 2003 Relationship between particle mass and mobility for diesel exhaust particles *Environ. Sci. Technol.* **37** 577–83

[12] Park K, Kittelson D B, Zachariah M R and McMurry P H 2004 Measurement of inherent material density of nanoparticle agglomerates *J. Nanopart. Res.* **62** 267–72

[13] Cox R G 1970 The motion of long slender bodies in a viscous fluid: Part 1. General theory *J. Fluid Mech.* **44** 791–810

[14] DeCarlo P E, Slowik J G, Worsnop D R, Davidovits P and Jimenez J L 2004 Particle morphology and density characterization by combined mobility and aerodynamic diameter measurements. Part 1: theory *Aerosol Sci. Technol.* **38** 1185–204

[15] Zelenyuk A, Cai Y and Imre D 2006 From agglomerates of spheres to irregularly shaped particles: determination of dynamic shape factors from measurements of mobility and vacuum aerodynamic diameters *Aerosol Sci. Technol.* **40** 197–217

[16] Emery M S 2005 Theoretical analysis of data from DMA-APM system *Master Thesis* University of Minnesota

[17] Schmidt-Ott A, Baltensperger U, Gaggeler H W and Jost D T 1990 *J. Aerosol Sci.* **21** 711–7

[18] Fuchs N A 1964 *The Mechanics of Aerosols* (New York: Dover) p 38

[19] Baron P A, Sorensen C M and Brockman J E 2001 Nonspherical particle measurements: shape factors, fractals, and fibers *Aerosol Measurement: Principles, Techniques, and Applications* 2nd edn, ed P A Baron and K Willeke (NewYork: Wiley) pp 705–49

[20] Knutson E O and Whitby K T 1975 Aerosol classification by electric mobility: apparatus, theory, and applications *J. Aerosol Sci.* **6** 443–51

[21] Ku B K and Maynard A D 2005 Comparing aerosol surface-area measurement of monodisperse ultrafine silver agglomerates using mobility analysis, transmission electron microscopy and diffusion charging *J. Aerosol Sci.* **36** 1108–24

[22] Ehara K, Hagwood C and Coakley K J 1996 Novel method to classify aerosol particles according to their mass-to-charge ratio-aerosol particle mass analyzer *J. Aerosol Sci.* **27** 217–34

[23] Maynard A D and Kuempel E D 2005 Airborne nanostructured particles and occupational health *J. Nanopart. Res.* **7** 587–614